Inverse Scattering of Inhomogeneous Dielectric Cylinders Buried in a Slab Medium by TE Wave Illumination

C. H. Huang, C. C. Chiu, C. J. Lin, and Y. F. Chen

Electrical Engineering Department, Tamkang University
Tamsui, Taipei, R.O.C.

Abstract **–** The inverse scattering of inhomogeneous dielectric cylinders buried in a slab medium by transverse electric (TE) wave illumination is investigated. Dielectric cylinders of unknown permittivities are buried in second space and scattered a group of unrelated waves incident from first space where the scattered field is recorded. By proper arrangement of the various unrelated incident fields, the difficulties of ill-posedness and nonlinearity are circumvented, and the permittivity distribution can be reconstructed through simple matrix operations. The algorithm is based on the moment method and the unrelated illumination method. Numerical results are given to demonstrate the capability of the inverse algorithm. Good reconstruction is obtained even in the presence of additive Gaussian random noise in measured data. In addition, the effect of noise on the reconstruction result is also investigated.

I. INTRODUCTION

In the last few years, inverse scattering problems of objects buried in slab medium have been a growing importance in many different fields of applied science, with a large potential impact on geosciences and remote sensing applications. Typical examples are the detection of water pipes buried in the wall, power and communication cables buried in the wall, archaeological remains and so on. However, the solutions are considerably more difficult than those involving objects in free space or a half space. This is due to the interaction between the air-earth interface and the object, which leads to the complicated Green's function for this three layer problem. Most microwave inverse scattering algorithms developed are for TM wave illuminations in which the vectorial problem can be simplified to a scalar one [1 - 10]. On the other hand, much fewer works have been reported on the more complicated TE case [11 - 17]. In the TE wave excitation case, the presence of polarization charges makes the inverse problem more nonlinear. As a result, the reconstruction becomes more difficult. However, the TE polarization case is useful because it provides additional information about the object. To the best of our knowledge, in TE case, there is still no investigation on the inverse scattering of inhomogeneous dielectric cylinders buried in a slab medium by unrelated illumination method.

In this paper, the inverse scattering of inhomogeneous dielectric cylinders buried in a slab medium by TE wave illumination is investigated. An efficient algorithm is proposed to reconstruct the permittivity distribution of the objects by using only the scattered field measured outside. The algorithm is based on the unrelated illumination method [9], [13], [15 - 16]. In section II, the theoretical formulation for electromagnetic inverse scattering is presented. Numerical results for objects of different permittivity distributions are given in section III. Finally, conclusions are drawn in section IV.

II. THEORETICAL FORMULATION

Let us consider dielectric cylinders buried in a lossless homogeneous half-space as shown in Fig. 1.

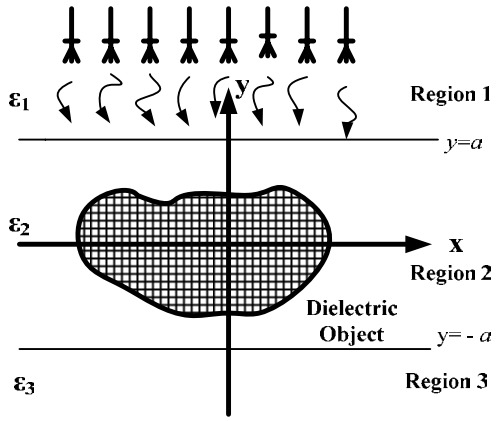

Fig. 1. Geometry of problem in the x-y plane.

$(\varepsilon_i, \sigma_i)$ $i = 1, 2, 3,$ denote the permittivities and conductivities in each region. The permeability is μ_0 for all material including the scatterers. The axis of the buried cylinder is the z-axis; that is, the properties of the scatterer may vary with the transverse coordinates only. A group of unrelated incident wave with magnetic field parallel to the z-axis (i.e., transverse electric, or TE, polarization) is illuminated upon the scatterers.

Owing to the interface, the incident plane wave

generates three waves that would exist in the absence of the conducting object. Let the unperturbed field be represented by

$$\vec{E}^i(x,y)=\begin{cases}\left(E_x^i\right)_1(x,y)\hat{x}+\left(E_y^i\right)_1(x,y)\hat{y}, & y\ge a,\\ \left(E_x^i\right)_2(x,y)\hat{x}+\left(E_y^i\right)_2(x,y)\hat{y}, & a>y>-a,\\ \left(E_x^i\right)_3(x,y)\hat{x}+\left(E_y^i\right)_3(x,y)\hat{y}, & y\le -a.\end{cases} \tag{1}$$

Using the vector potential techniques, the internal total electric field defined as

$$\vec{E}(x,y)=E_x(x,y)\hat{x}+E_y(x,y)\hat{y}=(E_x^i+E_x^s)\hat{x}+(E_y^i+E_y^s)\hat{y}$$

and the external scattered field,

$$\vec{E}^s(x,y)=E_x^s(x,y)\hat{x}+E_y^s(x,y)\hat{y}$$

can be expressed by the following equations,

$$E_x(\vec{r})=-\left(\frac{\partial^2}{\partial x^2}+k_2^2\right)\left[\int_s G(\vec{r},\vec{r}')(\varepsilon_1(\vec{r}')-1)E_x(\vec{r}')ds'\right]$$
$$-\frac{\partial^2}{\partial x\partial y}\left[\int_s G(\vec{r},\vec{r}')(\varepsilon_2(\vec{r}')-1)E_y(\vec{r}')ds'\right]+E_x^i(\vec{r}), \tag{2}$$

$$E_y(\vec{r})=-\frac{\partial^2}{\partial x\partial y}\left[\int_s G(\vec{r},\vec{r}')(\varepsilon_1(\vec{r}')-1)E_x(\vec{r}')ds'\right]$$
$$-\left(\frac{\partial^2}{\partial y^2}+k_2^2\right)\left[\int_s G(\vec{r},\vec{r}')(\varepsilon_2(\vec{r}')-1)E_y(\vec{r}')ds'\right]+E_y^i(\vec{r}), \tag{3}$$

$$E_x^s(\vec{r})=-\left(\frac{\partial^2}{\partial x^2}+k_2^2\right)\left[\int_s G(\vec{r},\vec{r}')(\varepsilon_1(\vec{r}')-1)E_x(\vec{r}')ds'\right]$$
$$-\frac{\partial^2}{\partial x\partial y}\left[\int_s G(\vec{r},\vec{r}')(\varepsilon_2(\vec{r}')-1)E_y(\vec{r}')ds'\right], \tag{4}$$

$$E_y^s(\vec{r})=-\frac{\partial^2}{\partial x\partial y}\left[\int_s G(\vec{r},\vec{r}')(\varepsilon_1(\vec{r}')-1)E_x(\vec{r}')ds'\right]$$
$$-\left(\frac{\partial^2}{\partial y^2}+k_2^2\right)\left[\int_s G(\vec{r},\vec{r}')(\varepsilon_2(\vec{r}')-1)E_y(\vec{r}')ds'\right], \tag{5}$$

with

$$G(x,y;x',y')=\begin{cases}G_{1s}(x,y:x',y'), & y\ge a,\\ G_{2s}(x,y;x',y'), & -a<y<a,\\ G_{3s}(x,y;x',y'), & y\le -a,\end{cases} \tag{6a}$$

$$G_{1s}(x,y;x',y')=\frac{1}{2\pi}\int_{-\infty}^{\infty}je^{-j\gamma_1(y-a)}$$
$$\frac{\left(\left(\gamma_2+\gamma_3\right)e^{j\gamma_2(y'+a)}+\left(\gamma_2-\gamma_3\right)e^{-j\gamma_2(y'+a)}\right)\times e^{-j\alpha(x-x')}}{\left(\gamma_1+\gamma_2\right)\left(\gamma_2+\gamma_3\right)e^{j\gamma_2(2a)}+\left(\gamma_1-\gamma_2\right)\left(\gamma_2-\gamma_3\right)e^{-j\gamma_2(2a)}}d\alpha, \tag{6b}$$

$$G_{2s}(x,y;x',y')=G_{2sf}(x,y;x',y')+G_{2ss}(x,y;x',y'), \tag{6c}$$

$$G_{3s}(x,y;x',y')=\frac{1}{2\pi}\int_{-\infty}^{\infty}je^{j\gamma_1(y+a)}$$
$$\frac{\left(\left(\gamma_1+\gamma_2\right)e^{-j\gamma_2(y'-a)}+\left(\gamma_2-\gamma_1\right)e^{j\gamma_2(y'-a)}\right)\times e^{-j\alpha(x-x')}}{\left(\gamma_1+\gamma_2\right)\left(\gamma_2+\gamma_3\right)e^{j\gamma_2(2a)}+\left(\gamma_1-\gamma_2\right)\left(\gamma_2-\gamma_3\right)e^{-j\gamma_2(2a)}}d\alpha, \tag{6d}$$

where

$$G_{2sf}(x,y;x',y')=\frac{j}{4}H_0^{(2)}\left(k_2\sqrt{(x-x')^2+(y-y')^2}\right),$$

$$G_{2ss}(x,y,x',y')=$$
$$\frac{1}{2\pi}\times\int_{-\infty}^{\infty}\frac{je^{-j\alpha(x-x')}}{2r_2}\left\{\left[\frac{(r_2-r_1)(r_2-r_3)\left[e^{-jr_2\left[|y-y'|+2a\right]}+e^{jr_2\left[|y-y'|-2a\right]}\right]}{(r_1+r_2)(r_2+r_3)e^{jr_2(2a)}+(r_1-r_2)(r_2-r_3)e^{-jr_2(2a)}}\right]\right.$$
$$\left.+\left[\frac{(r_2-r_1)(r_2+r_3)e^{jr_2\left(y+y'\right)}+(r_2-r_3)(r_1+r_2)e^{-jr_2\left(y+y'\right)}}{(r_1+r_2)(r_2+r_3)e^{jr_2(2a)}+(r_1-r_2)(r_2-r_3)e^{-jr_2(2a)}}\right]\right\}d\alpha$$

$\gamma_i^2=k_i^2-\alpha^2$, $i=1,\ 2,\ 3$, $\mathrm{Im}(r_i)\le 0$, $-a<y'<a$.

Here, k_i denotes the wave number in region i and ε_r is the relative permittivity of the dielectric objects. $G(x,y;x',y')$ is the Green's function, which can be obtained by the Fourier transform [18]. For numerical implementation of Green's function, we might face some difficulties in calculating this function. This Green's function is in the form of an improper integral, which must be evaluated numerically. However, the integral converges very slowly when (x,y) and (x',y') approach the interface $y=a$. Fortunately we find that the integral in G_{1s}, G_{2s}, and G_{3s} may be rewritten as a closed-form term plus a rapidly converging integral [2]. Thus, the whole integral in the Green's function can be calculated efficiently.

The direct scattering problem is to calculate the scattered field $\vec{E}^s$ in region 1, while the permittivity distribution of the buried objects is given. This can be achieved by first solving the total field $\vec{E}$ in equations (2) and (3) as well as calculating $\vec{E}^s$ in equations (4) and (5). For numerical implementation of the direct problem, the dielectric objects are divided into *N* sufficient small cells. Thus the permittivity and the total field within each cell can be taken as constants. Then the moment method is used to solve equations (2) to (5) with a pulse basis function for expansion and point matching for testing [19]. Equations (2) to (5) can then be transformed into a matrix form

$$\begin{pmatrix}E_x^i\\ E_y^i\end{pmatrix}=\left\{\begin{bmatrix}[G_1] & [G_2]\\ [G_2] & [G_3]\end{bmatrix}\begin{bmatrix}[\tau] & 0\\ 0 & [\tau]\end{bmatrix}+\begin{bmatrix}[I] & 0\\ 0 & [I]\end{bmatrix}\right\}\begin{pmatrix}E_x\\ E_y\end{pmatrix}, \tag{7}$$

$$\begin{pmatrix} E_x^s \\ E_y^s \end{pmatrix} = \left\{ -\begin{bmatrix} [G_4] & [G_5] \\ [G_5] & [G_6] \end{bmatrix} \begin{bmatrix} [\tau] & 0 \\ 0 & [\tau] \end{bmatrix} \right\} \begin{pmatrix} E_x \\ E_y \end{pmatrix}, \quad (8)$$

where (E_x^i) and (E_y^i) represent the N-element incident field column vectors and, (E_x) and (E_y) are the N-element total field column vectors. (E_x^s) and (E_y^s) denote the M-element scattered field column vectors. Here, M is the number of measurement points. The matrices [G_1], [G_2], and [G_3] are $N \times N$ square matrices. [G_4], [G_5], and [G_5] are $M \times N$ matrices. The element in matrices [G_i], i =1, 2, 3…6 can be obtained by tedious mathematic manipulation (see Appendix). [τ] is a $N \times N$ diagonal matrix whose diagonal element are formed from the permittivities of each cell minus one. [I] is an identity $N \times N$ matrix.

For the inverse scattering problem, the permittivity distribution of the dielectric objects is to be computed by the knowledge of the scattered field measured in region 1. In the inversion procedure, 2N different incident column vectors are used to illuminate the object, the follow equations are obtained,

$$[E_t^i] = [[G_{t1}][\tau_t] + [I_t]] \ [E_t], \quad (9)$$

$$[E_t^s] = -[G_{t2}] \ [\tau_t] \ [E_t] \quad (10)$$

where

$$[E_t^i] = \begin{bmatrix} E_x^i \\ E_y^i \end{bmatrix}, \quad [E_t] = \begin{bmatrix} E_x \\ E_y \end{bmatrix}, \quad [E_t^s] = \begin{bmatrix} E_x^s \\ E_y^s \end{bmatrix},$$

$$[G_{t1}] = \begin{bmatrix} [G_1] & [G_2] \\ [G_2] & [G_3] \end{bmatrix}, [G_{t2}] = \begin{bmatrix} [G_4] & [G_5] \\ [G_5] & [G_6] \end{bmatrix}$$

$$[\tau_t] = \begin{bmatrix} [\tau] & 0 \\ 0 & [\tau] \end{bmatrix}, \quad [I_t] = \begin{bmatrix} [I] & 0 \\ 0 & [I] \end{bmatrix},$$

Here, $[E_t^i]$ and $[E_t]$ are both $2N \times 2N$ matrices. $[E_t^s]$ is an $M \times 2N$ matrix. It is worth mentioning that other than matrix $[G_{t2}]$, the matrix $[G_{t1}][\tau_t] + [I_t]$ is always a well-posed one in any case, therefore we can first solve $[E_t^i]$ in equation (9) and substitute into equation (10), and then [τ_t] can be found by the following equation

$$[\Psi_t][\tau_t] = [\Phi_t] \quad (11)$$

where

$$[\Phi_t] = -[E_t^s][E_t^i]^{-1}$$

$$[\Psi_t] = [E_t^s][E_t^i]^{-1}[G_{t1}] + [G_{t2}]$$

From equation (11), all the diagonal elements in the matrix [τ] can be determined by comparing the element with the same subscripts which may be any row of both $[\Psi_t]$ and $[\Phi_t]$,

$$(\tau)_{nn} = \frac{(\Phi_t)_{mn}}{(\Psi_t)_{mn}}, \quad n \le N \quad (12a)$$

or

$$(\tau)_{(n-N)(n-N)} = \frac{(\Phi_t)_{mn}}{(\Psi_t)_{mn}}, \quad n \ge N+1. \quad (12b)$$

Then the permittivities of each cell can be obtained as follow,

$$\varepsilon_n = (\tau)_{nn} + 1. \quad (13)$$

Note that there are a total of 2M possible values for each element of τ. Therefore, the average value of these 2M data is computed and chosen as final reconstruction result in the simulation.

In the above derivation, the key problem is that the incident matrices $[E_t^i]$ must not be a singular matrix, i.e., all the incident column vectors that form the $[E_t^i]$ matrices, must be linearly unrelated. Thus, if the object is illuminated by a group of unrelated incident waves, it is possible to reconstruct the permittivity distribution of the objects. Note that when the number of cells becomes very large; it is difficult to make such a great number of independent measurements. In such a case, some regularization methods must be used to overcome the ill-posedness

III. NUMERICAL RESULTS

In this section, we report some numerical results obtained by computer simulations using the method described in section II. Consider a lossless three- layer structure ($\sigma_1 = \sigma_2 = \sigma_3 = 0$) and the width of the second layer is 0.2m. The permittivity in each region is characterized by $\varepsilon_1 = \varepsilon_0$, $\varepsilon_2 = 2.25\varepsilon_0$ and $\varepsilon_3 = \varepsilon_0$, respectively, as shown in Fig. 1. The frequency of the incident wave is chosen to be 3 GHz. The incident waves are generated by numerous groups of radiators operated simultaneously.

Each group of radiators is restricted to transmit a narrow-bandwidth pattern that can be implemented by antenna array techniques. By changing the beam direction and tuning the phase of each group of radiators, one can focus all the incident beams in turn at each cell of the object. This procedure is known as *Beam Focusing* [9]. Note that this focusing should be set when the scatterer is absent. Clearly, an incident matrix formed in this way is diagonally dominant and its inverse matrix exists. The measurement is taken from 0.4 m to -0.4 m in region 1 at equal spacing. The number of measurement points is set to be 9 for each illumination. For avoiding trivial inversion of finite dimensional problems, the discretization number for the direct problem is four times that for the inverse problem in our numerical simulation.

In the first example, the buried cylinder with a 70 ×

21 mm rectangular cross section is discretized into 20 × 6 cells, and the corresponding dielectric permittivities are plotted in Fig. 2. The model is characterized by simple step distribution of permittivity. Each cell has 3.5 × 3.5 mm cross-sections. The reconstructed permittivity distributions of the object are plotted in Fig. 3. The root-mean-square (RMS) error is about 0.9 %. It is apparent that the reconstruction is good.

In the second example, the buried cylinder with a 36 × 36 mm square cross section is discretized into 10 × 10 cells, and the corresponding dielectric permittivities are plotted in Fig. 4. The model is characterized by a four-layer contrast of permittivity. Each cell has 3 × 3 mm cross-sections. The reconstructed permittivity distributions of the object are plotted in Fig. 5. The root-mean-square (RMS) error is about 1.21 %. We can see the reconstruction is also good.

For investigating the effect of noise, we add to each complex scattered field a quantity b+cj,

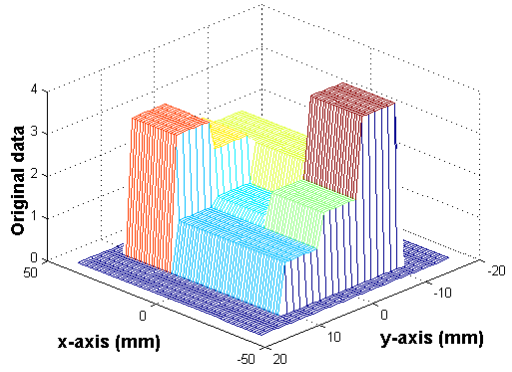

Fig. 2. Original relative permittivity distribution for example 1.

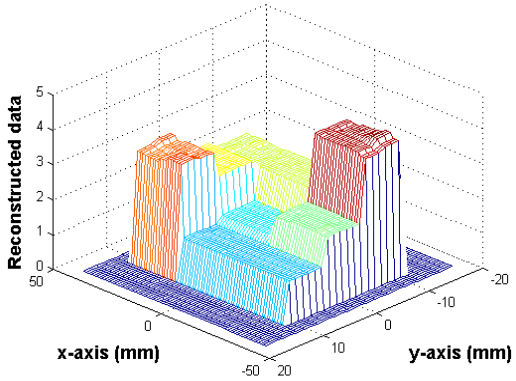

Fig. 3. Reconstructed relative permittivity distribution for example 1.

where b and c are independent random numbers having a Gaussian distribution over 0 to the noise level times the RMS value of the scattered field. The noise levels applied include 10^{-5}, 10^{-4}, 10^{-3}, 10^{-2}, and 10^{-1} in the simulations. The numerical results for examples 1 and 2 are plotted in Figs. 6 and 7, respectively. They show the effect of noise is tolerable for noise levels below 1%.

Our method depends on the condition number of $[E_t^i]$; that is, on having 2N unrelated measurements. The procedure will generally not work when the number of unknowns gets very large. This is due to the fact that it is difficult to make such a great number of measurements and make them all unrelated. As a result, the condition number of $[E_t^i]$ will become large while the number of unknowns is very large. In such a case, the regularization method should be employed to overcome the ill-posedness. For instance, the pseudoinverse transform techniques [7] can be applied for the inversion of the $[E_t^i]$ matrix.

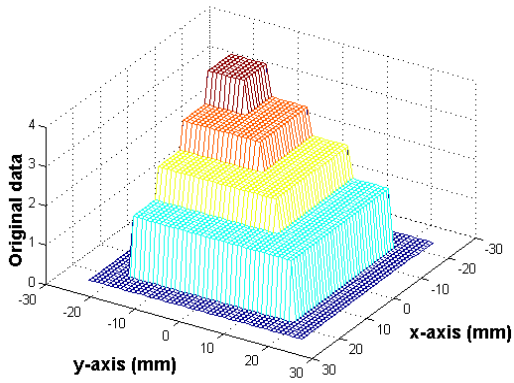

Fig. 4. Original relative permittivity distribution for example 2.

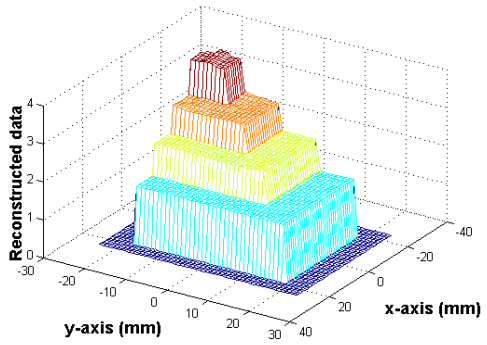

Fig. 5. Reconstructed relative permittivity distribution for example 2.

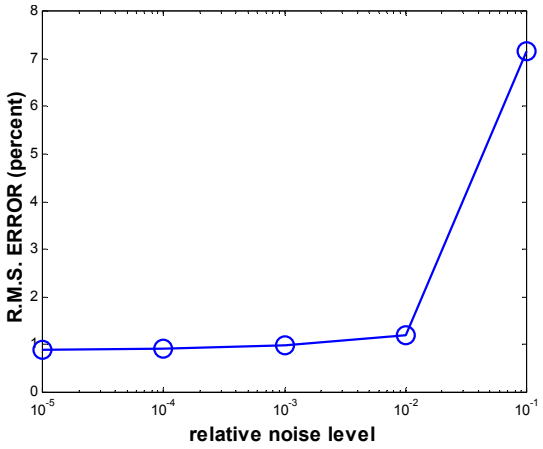

Fig. 6. Reconstructed error as a function of noise level for example 1.

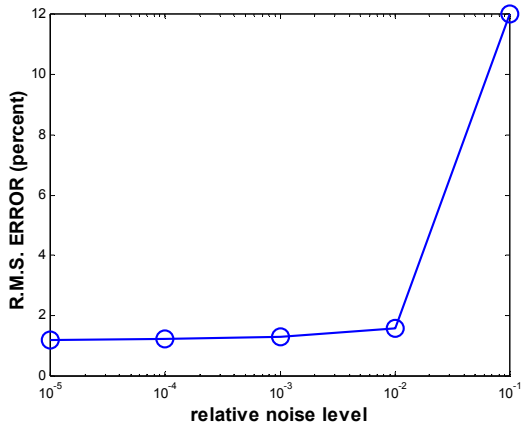

Fig. 7. Reconstructed error as a function of noise level for example 2.

IV. CONCLUSIONS

Imaging algorithm for TE case is more complicated than that for the TM case, due to the added difficulties in the polarization charges. Nevertheless, the polarization charges cannot be ignored for this two-dimensional problem and all three-dimensional problems. In this paper, an efficient algorithm for reconstructing the permittivity distribution of inhomogeneous dielectric cylinders buried in a slab medium, illuminated by TE waves, has been proposed. By properly arranging the direction of various unrelated waves, the difficulty of ill-posedness and nonlinearity is avoided. Thus, the permittivity distribution can be obtained by simple matrix operations. The moment method has been used to transform a set of integral equations into matrix form. Then these matrix equations are solved by the unrelated illumination method. Numerical simulation for imaging the permittivity distribution of an inhomogeneous dielectric cylinder buried in a slab medium has been carried out and good reconstruction has been obtained even in the presence of Gaussian noise in measured data. This algorithm is very effective and efficient, since no iteration is required.

APPENDIX

The element in the matrix $[G_1]$ can be written as

$$(G_3)_{mn} = \left[\left(\frac{\partial^2}{\partial x^2} + k_2^2\right)\cdot \iint_{cell\ n} G_2(x,y;x',y')dx'dy'\right]\Bigg|_{\substack{x=x_m\\y=y_m}}$$

where (x_m, y_m) is the observation point located in the center of the mth cell. For a sufficient small cell, we can replace the cell by a circular cell with the same cross section [20]. Let the equivalent radius of the nth circular cell be a_n. The $(G_1)_{mn}$ can be expressed in the following form

$$(G_3)_{mn} = \begin{cases} \left.\dfrac{\partial^2 G_s(x,y;x_n,y_n)}{\partial x^2}\right|_{\substack{x=x_m\\y=y_m}}\cdot\Delta S_n \\ +G_s(x_m,y_m;x_n,y_n)\cdot k_2^2\cdot\Delta S_n \\ +\dfrac{j\pi a_n J_1(k_2 a_n)}{2\rho_{mn}^3}k_2\rho_{mn}(y_m-y_n)^2 H_0^{(2)}(k_2\rho_{mn}) \\ +\left((x_m-x_n)^2-(y_m-y_n)^2\right)H_1^{(2)}(k_2\rho_{mn}), \quad m\neq n \\ \left.\dfrac{\partial^2 G_s(x,y;x_n,y_n)}{\partial x^2}\right|_{\substack{x=x_m\\y=y_m}}\cdot\Delta S_n \\ +G_s(x_m,y_m;x_n,y_n)\cdot k_2^2\cdot\Delta S_n \\ +\dfrac{j}{4}\left[\pi k_2 a_n H_1^{(2)}(k_2 a_n)-4j\right], \quad m=n \end{cases}$$

with $\rho_{mn} = \sqrt{(x_m-x_n)^2+(y_m-y_n)^2}$, where J_1 is Bessel function of the first order and (x_n, y_n) is the center of the cell n. ΔS_n denotes the area of the nth cell. Similarly,

$$(G_2)_{mn} = \begin{cases} \left.\dfrac{\partial^2 G_{2ss}(x,y;x_n,y_n)}{\partial x\partial y}\right|_{\substack{x=x_m\\y=y_m}}\cdot\Delta S_n \\ +\dfrac{j\pi a_n J_1(k_2 a_n)}{2\rho_{mn}^3}(x_m-x_n)(y_m-y_n)\times \\ 2H_1^{(2)}(k_2\rho_{mn})-k_2\rho_{mn}H_0^{(2)}(k_2\rho_{mn}), \quad m\neq n \\ 0, \quad m=n \end{cases}$$

$$
\left(G_3\right)_{mn}=\begin{cases}
\left.\dfrac{\partial^2 G_{2ss}\left(x,y;x_n,y_n\right)}{\partial y^2}\right|_{\substack{x=x_m\\ y=y_m}}\cdot\Delta S_n \\
+G_{2ss}\left(x_m,y_m;x_n,y_n\right)\cdot k_2^2\cdot\Delta S_n \\
+\dfrac{j\pi a_n J_1\left(k_2 a_n\right)}{2\rho_{mn}^3} \\
\times\begin{bmatrix} k_2\rho_{mn}\left(x_m-x_n\right)^2 \\ \times H_0^{(2)}\left(k_2\rho_{mn}\right) \\ +\begin{pmatrix}\left(y_m-y_n\right)^2 \\ -\left(x_m-x_n\right)^2\end{pmatrix} \\ \times H_1^{(2)}\left(k_2\rho_{mn}\right)\end{bmatrix}, & m\neq n \\
\left.\dfrac{\partial^2 G_{2ss}\left(x,y;x_n,y_n\right)}{\partial y^2}\right|_{\substack{x=x_m\\ y=y_m}}\cdot\Delta S_n \\
+G_{2ss}\left(x_m,y_m;x_n,y_n\right)\cdot k_2^2\cdot\Delta S_n \\
+\dfrac{j}{4}\left[\pi k_2 a_n H_1^{(2)}\left(k_2 a_n\right)-4j\right], & m=n
\end{cases}
$$

$$
\left(G_4\right)_{mn}=\left.\frac{\partial^2 G_{1s}\left(x,y;x_n,y_n\right)}{\partial x^2}\right|_{\substack{x=x_m\\ y=y_m}}\cdot\Delta S_n + G_{1s}\left(x_m,y_m;x_n,y_n\right)\cdot k_2^2\cdot\Delta S_n \quad ,
$$

$$
\left(G_5\right)_{mn}=\left.\frac{\partial^2 G_{1s}\left(x,y;x_n,y_n\right)}{\partial x^2}\right|_{\substack{x=x_m\\ y=y_m}}\cdot\Delta S_n + G_{1s}\left(x_m,y_m;x_n,y_n\right)\cdot k_2^2\cdot\Delta S_n \quad ,
$$

$$
\left(G_6\right)_{mn}=\left.\frac{\partial^2 G_{1s}\left(x,y;x_n,y_n\right)}{\partial y^2}\right|_{\substack{x=x_m\\ y=y_m}}\cdot\Delta S_n + G_{1s}\left(x_m,y_m;x_n,y_n\right)\cdot k_2^2\cdot\Delta S_n \quad .
$$

REFERENCES

[1] S. Caorsi, G.L. Gragnani, and M. Pastorino, "Numerical electromagnetic inverse-scattering solution for two-dimensional infinite dielectric cylinders buried in a lossy half-space," *IEEE Trans. Antennas Propagat.*, vol. AP-41, pp. 352 - 356, Feb. 1993.

[2] C. C. Chiu and Y. M. Kiang, "Inverse scattering of a buried conducting cylinder," *Inv. Prob.*, vol. 7, pp. 187 - 202, April 1991.

[3] C. C. Chiu and C. P. Huang, "Inverse scattering of dielectric cylinders buried in a half space," *Microwave and Optical Technology Letters*, vol. 13, pp. 96 - 99, Oct. 1996.

[4] F. Soldovieri and R. Persico, "Reconstruction of an embedded slab from multifrequency scattered field data under the distorted born approximation", *IEEE Trans. Antennas Propagat.*, vol. 52, pp. 2348 - 2356, Sept. 2004.

[5] O. M. Bucci, L. Crocco, T. Isernia, and V. Pascazio, "Inverse scattering problems with multifrequency data: reconstruction capabilities and solution strategies," *IEEE Trans. Geoscience and Remote Sensing*, vol. 38, pp. 1749 - 1756, July 2000.

[6] V. A. Mikhnev and P. Vainikainen, "Two-step inverse scattering method for one-dimensional permittivity profiles," *IEEE Trans. Antennas Propagat.*, vol. 48, pp. 293 - 298, Feb. 2000.

[7] M. M. Ney, A. M. Smith, and S. S. Stuchly, "A solution of electromagnetic imaging using pseudoinverse transformation," *IEEE Trans. Med. Imag.*, vol. MI-3, pp. 155 - 162, Dec. 1984.

[8] S. Caorsi, G. L. Gragnani, and M. Pastorino, "An approach to microwave imaging using a multiview Moment Method solution for a two-dimensional infinite cylinder," *IEEE Trans. Microwave Theory and Techniques*, vol. MTT-39, pp. 1062 - 1067, June 1991.

[9] W. Wang and S. Zhang, "Unrelated illumination method for electromagnetic inverse scattering of inhomogeneous lossy dielectric bodies," *IEEE Trans. Antennas Propagat.*, vol. AP-40, pp. 1292 - 1296, Nov. 1992.

[10] K. A. Nabulsi and D. G. Dudley, "A new approximation and a new measurable constraint for slab profile inversion," *IEEE Trans. on Geoscience and Remote Sensing*, vol. 34, no. 3, May 1996.

[11] N. Joachimowicz, C. Pichot, and J. P. Hugonin, "Inverse scattering: an iterative numerical method for electromagnetic imaging," *IEEE Trans. Antennas Propagat.*, vol. AP-39, pp. 1742 - 1752, Dec. 1991.

[12] G. P. Otto and W. C. Chew, "Inverse scattering of Hz waves using local shape function imaging: a T-Matrix formulation," *Int. J. Imaging Syst.*

Technol., vol. 5, pp. 22 - 27, 1994.
[13] C. C. Chiu and P. T. Liu, "Image reconstruction of a complex cylinder illuminated by TE waves," *IEEE Trans. Microwave Theory Tech.*, vol. 44, pp. 1921 - 1927, Oct. 1996.
[14] C. P. Chou and Y. W. Kiang, "Inverse scattering of dielectric cylinders by a cascaded TE-TM method," *IEEE Trans. Microwave Theory and Techniques*, pp. 1923 - 1930, vol. 47, Oct. 1999.
[15] C. C. Chiu and C. J. Lin, "Image reconstruction of buried uniaxial dielectric cylinders," *Journal of Electromagnetic Waves and Applications*, vol. 22, no. 2, pp. 97 - 112, Feb. 2002.
[16] C. C. Chiu and C. J. Lin, "Image reconstruction of buried dielectric cylinders by TE wave illumination," *Journal of Electromagnetic Waves and Applications*, vol. 16, no. 2, pp. 243 - 245, Feb. 2002.
[17] B. J. Kooij, "Contrast source inversion of a buried object in TE-scattering," *Antennas and Propagation Society International Symposium*, vol. 2, pp. 714 - 717, June 1998.
[18] J. R. Wait, *Electromagnetic Waves in Stratified Media,* Macmillan, New York, 1962.
[19] R. F. Harrington, "Field Computation by Moment Methods," *New York: Macmillan*, 1968.
[20] J. H. Richmond, "TE-wave scattering by a dielectric cylinder of arbitrary cross-session shape," *IEEE Trans. Antennas Propagat.*, vol. 14, pp. 460 - 464, July 1966.

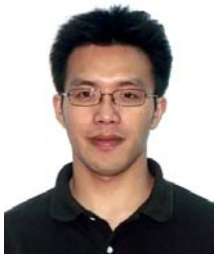

Chung-Hsin Huang was born in Tucheng, Taiwan, Republic of China, on February 1, 1980. He is currently working toward Ph.D. degree in the Department of Electrical Engineering, Tamkang University. His current research interests include numerical techniques in electromagnetics and indoor wireless communications.

Chien-Ching Chiu was born in Taoyuan, Taiwan, Republic of China, on January 23, 1963. He received the B.S.C.E. degree from National Chiao Tung University, Hsinchu, Taiwan, in 1985 and M.S.E.E. and Ph.D degrees from National Taiwan University, Taipei, Taiwan, in 1987 and 1991, respectively. From 1987 to1989, he served in the ROC Army Force as a communication officer. In 1992 he joined the faculty of the Department of Electrical Engineering, Tamkang University, where he is now an Professor. He was a visiting scholar at the MIT and University of Illinois, Urbana from 1998 to 1999. His current research interests include microwave imaging, numerical techniques in electromagnetics and indoor wireless communications.

Chun Jen Lin was born in Tamsui, Taiwan, Republic of China, on February 19, 1977. He is now a graduate student in the Department of Electrical Engineering, Tamkang University. His current research interests include numerical techniques in electromagnetics and indoor wireless communications

Ying-Feng Chen was born in Chai-Yi, Taiwan, Republic of China, on August 13, 1982. He is currently working toward M.S.E.E. degree in the Department of Electrical Engineering, Tamkang University. His current research interests include numerical techniques in electromagnetics and indoor wire less communications.